Research on Dead Time Optimization Characteristics of High-Power Three-Phase LLC Resonant Converter

Xianjin HUANG, Hongchao BAI, Zhidong XUE, Yinghui ZHAO, Wenwen SHI, and Linfeng ZHAO

***Abstract*—Reasonable dead time is a prerequisite for realizing zero-voltage turn-on (ZVS) of IGBT in a three-phase LLC converter. At the same time, the operating temperature greatly affects the output capacitance characteristics of IGBT. When the operating temperature of the IGBT rises, it will result in the dead time that has been set is no longer appropriate, thus making the IGBT lose the soft-switching operating characteristics. To address this problem, the article analyzes the soft-switching realization conditions of the three-phase LLC converter and studies the relationship between the soft-switching realization and the dead time. The shutdown characteristics of IGBTs at different operating temperatures are analyzed. It is found that the higher the operating junction temperature of IGBTs in three-phase LLC resonant circuits, the more unfavorable it is to realize soft switching, and the formulas of the minimum dead time and the maximum dead time to ensure the zero-voltage turn-on of IGBTs at the worst operating temperatures are deduced. A 100 kW three-phase LLC converter prototype is constructed for verification. The soft switching can still be realized and the high efficiency can be maintained under the case of higher operating power, which verifies the accuracy of the dead time optimization design.**

***Index Terms*—Dead time, IGBT, soft switching, three-phase LLC resonant converter.**

I. Introduction

The LLC resonant converter has the advantages of high efficiency, lightweight, small size, and soft-switching characteristics, and is capable of realizing zero-voltage switching (ZVS) conduction of the primary-side switching tube and zero-current switching (ZCS) turn-off of the secondary-side rectifier diode within the full-load range, which greatly improves the efficiency of the converter[1]−[3].To meet the high-power, high-current output requirements, the LLC resonant converter can be a multi-phase staggered parallel connection, the structure on the one hand, can reduce the current stress of each phase of the switching device of the LLC resonant converter, reduce its loss, on the other hand, can reduce the ripple in the output current, improve the service life of the filter capacitor [4]−[8]. In practice, a three-phase LLC converter needs to be controlled with a dead time to maintain the effective turn-off signal until the other switch in the same bridge arm is completely turned off to avoid the occurrence of the two switching tubes in the same bridge arm going straight through [9]. To realize the soft-switching operation of the primary switching tube, the converter needs to operate in the inductive region and the resonant current of the resonant network must be large enough to ensure that the parasitic capacitance of the primary switching tube and the secondary rectifier diode is fully charged and discharged within the dead time [10]. The dead time setting is very important for realizing soft switching and is determined by the parasitic capacitance of the primary-side switching tube and the resonance parameters of the converter. In conventional parametric design, the junction capacitance of the IGBT is often converted to a definite value when determining the dead time, but in practice, the IGBT output capacitance is affected by the voltages at the C- and E-pole terminals and the operating temperature of the IGBT [11]. [12] proposed an efficiency-optimized dead time and excitation inductance design to find the efficiency-optimized dead time design by deriving the relationship between the switching tube loss and the minimum dead time that can satisfy the soft-switching case. The effect of power switching tube junction capacitance variation with the operating environment is not considered. [13] analyzes the principle of selecting the dead time of the LLC converter to realize ZVS in a wide regulation range and uses the data in the MOSFET manual to calculate the minimum value of the dead time of the LLC converter to realize ZVS under the worst operating conditions without considering the effects of the converter's operating power and the switching tube's operating temperature on the switching tube. [14] considered the effect of different operating states of the LLC converter on the dead time and determined the maximum value of the dead time under extreme operating conditions, but did not analyze the minimum dead time. [15] proposed an adaptive deadband modulation scheme, which no longer needs to calculate the deadband time so that the deadband time changes dynamically with the operating conditions to realize soft switching, but the control design is more complex and may affect the performance of the LLC converter using other control methods. [16] proposed a dead time design method considering various controllable factors

Manuscript received December 17, 2024; revised February 28, 2025; accepted March 27, 2025. Date of publication June 30, 2025; date of current version April 18, 2025. This work was supported in part by Intellectual Property Licensing Program under the grant E24ZH200040. *(Corresponding author: Xianjin huang.)*

X. Huang, Z. Xue, and L. Zhao are with the School of Electrical Engineering, Beijing Jiaotong University, Beijing 100044, China (e-mail: xianjinhuang@bjtu.edu.cn; 22121539@bjtu.edu.cn; 23126403@bjtu.edu.cn).

H. Bai, Y. Zhao, and W. Shi are with Shandong Ainuo Instrument Co., Ltd, Jinan 215008, China (e-mail: 81202766@ainuo.com; dcm@ainuo.com; psmd@ainuo.com).

Digital Object Identifier 10.24295/CPSSTPEA.2025.00017

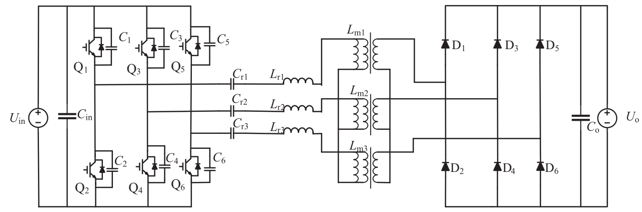

Fig. 1. Three-phase LLC resonant converter topology.

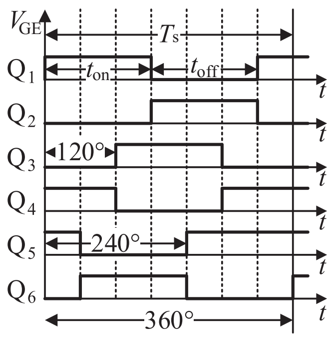

Fig. 2. gate signal.

and noise factors in the LLC resonant circuit, the main principle is to use the Monte Carlo method to simulate the fluctuation characteristics and fluctuation contribution rate of the dead time range, and to optimize the calculated dead time range, but the method requires a large amount of data as a support, and the design process is very cumbersome. [17] proposed a zero-voltage analysis and dead-time design of a half-bridge LLC-DCX converter considering nonlinear capacitance and different load values, analyzed in detail the charging and discharging process of the output capacitance during the dead-time and gave the dead-time formula considering nonlinear capacitance and different load values, but the design process is relatively cumbersome and the analysis is not comprehensive enough, and the junction capacitance is not analyzed from the characteristics of the power switching tubes to analyze the effect of the dead-time. The effect of junction capacitance on the dead time is not analyzed from the characteristics of the power switching tube.

In the high-power converter after a long period of operation of the IGBT module temperature produces a sharp change, this time if the dead time is set unreasonably, the power switching tube will lose the soft switching so that the converter efficiency is reduced, so it is necessary to amend the existing dead time design method. Based on the characteristics of the three-phase LLC circuit topology, this paper analyzes in detail the relationship between dead time and soft switching and obtains the dead time range formula, then analyzes the switching characteristics of the IGBT, studies in detail the relationship between the IGBT output capacitance and its junction temperature and the output load, and determines the size of the worst-case IGBT output capacitance, and makes corrections to the dead time range.

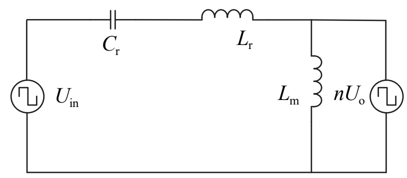

Fig. 3. Equivalent circuit at resonant frequency.

II. Three-Phase LLC Resonant Converter

A. Three-Phase LLC Resonant Converter Working Principle

The three-phase LLC resonant converter circuit topology is shown in Fig. 1, where Q_1~Q_6 are IGBTs, C_1~C_6 are the junction capacitances of the IGBTs, U_{in} is the input voltage, U_o is the output voltage, C_{in} is the input capacitance, C_o is the output capacitance, L_{r1}, L_{r2} and L_{r3} are the resonant inductances, L_{m1}, L_{m2} and L_{m3} are the excitation inductances, C_{r1}, C_{r2} and C_{r3} are the resonant capacitors and n is the transformer turns ratio. The three-phase LLC resonant converter is mainly composed of four parts: inverter bridge, resonant cavity, rectifier bridge and filter capacitor. Among them, in order to solve the problem of uneven power due to uneven current when there is a difference in parameters, the transformer's primary and secondary sides are Y-Y connected three-phase LLC resonant converters. The inverter bridge consists of six power switching tubes, the resonant cavity includes resonant inductor L_r, resonant capacitor C_r, and excitation inductance L_m, and the rectifier bridge consists of six diodes.

The three-phase LLC converter drive signals are shown in Fig. 2, and the three-phase PWM operates with a 120° phase difference between them [18].

B. Calculation of Resonant Current of Three-Phase LLC Resonant Converter

In the ideal case, the resonance parameters between the three phases of the three-phase bidirectional LLC resonant converter are exactly the same, so it can be analyzed as a single phase [19]. The first resonant frequency f_r and the second resonant frequency f_m are shown in (1) and (2). The operating modes of the three-phase LLC resonant converter can be categorized into four operating modes: $f_m < f_s < f_r$, $f_s = f_r$, $f_s > f_r$, and $f_s < f_m$.

$$f_r = \frac{1}{2\pi\sqrt{L_r C_r}} \tag{1}$$

$$f_m = \frac{1}{2\pi\sqrt{(L_m + L_r)C_r}} \tag{2}$$

Fig.3 shows the equivalent circuit of a three-phase LLC operating at the resonant frequency. As for the three-phase LLC converter, operating at the first resonant frequency can realize the ZVS of the primary switching tube and the ZCS of the secondary diode, which can obtain the highest efficiency,

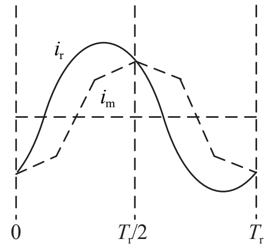

Fig. 4. The resonant current and magnetizing current.

and also can obtain the DC gain that does not change with the load. Moreover, when the switching frequency f_s is close to the resonant frequency f_r, the current in the resonant slot circuit is approximated as a sinusoidal waveform, so the fundamental waveform approximation can be used to simplify the converter into a linear circuit analysis, which can greatly reduce the difficulty of circuit analysis.

Fig. 4 shows the key current waveform of a three-phase LLC operating at the resonant frequency, where i_r is the resonant current and i_m is the excitation current. From Fig. 4, it can be seen that the resonant current at the resonant frequency has a sinusoidal waveform with the expression,

$$i_r = \sqrt{2} I_{\text{rms\_p}} \sin(\omega_r t + \theta) \tag{3}$$

where $I_{\text{rms\_p}}$ is the RMS value of the primary current, θ is the phase difference between the resonant current and the excitation inductor current, and ω_r is the angular frequency of the resonant frequency. From Fig. 4, it can be seen that the excitation current and resonant current are equal at one-half resonant cycle. At this time $i_{\text{m\_pk}}$ is the peak value of the excitation current and the magnitude is,

$$i_{\text{m\_pk}} = \frac{nU_o T_r}{9L_m} \tag{4}$$

where T_r is the resonance period resonance, the average value of the difference between the current and the excitation current is the average value of the output current converted to the primary side. So the following two equations are established,

$$i_r\left(\frac{T_r}{2}\right) = i_{\text{m\_pk}} \tag{5}$$

$$\frac{\int_0^{\frac{T_r}{2}} \left[i_r(t) - i_m(t)\right] \mathrm{d}t}{\frac{T_r}{2}} = \frac{nU_o}{3R_L} \tag{6}$$

where R_L is the output load, the expression for the RMS value of the primary current can be introduced from (5) and (6) as,

$$I_{\text{prms}} = \frac{U_o\sqrt{18\pi^2 L_m^2 + 2R_L^2 T_s^2 n^4}}{18 L_m R_L n} \tag{7}$$

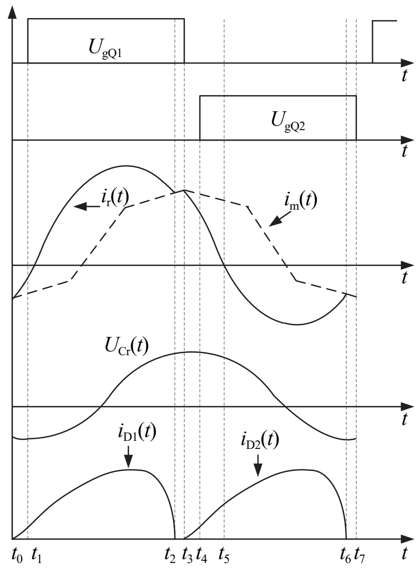

Fig. 5. The key waveform in the under-resonant state.

where T_s is the switching period, the secondary current is equivalent to the difference between the primary resonant current and the excitation current folded to the secondary current, then can get the RMS value of the secondary current as,

$$I_{\text{srms}} = \frac{\pi U_o}{3\sqrt{2} R_L} \tag{8}$$

III. Deadband Characterization of Three-Phase LLC Resonant Converter

A. Analysis of Soft-Switching Realization Conditions for LLC Resonant Converter

Generally when designing the LLC resonant converter the closer the switching frequency is to the resonant frequency, the higher the efficiency of the converter, so the switching frequency is usually chosen to be slightly less than the resonant frequency, to be able to realize the ZVS of the primary-side switching tube and the ZCS of the secondary-side diode, whose typical operating waveforms are shown in Fig. 5.

High-power three-phase LLC resonant converters generally use IGBT as a switching tube, and LLC converter IGBT to achieve soft switching prerequisite is that before the arrival of the drive signal, the voltage at both ends of the IGBT junction capacitance has dropped to 0. Let t_d be the dead time; ω_r be the angular frequency for the resonance frequency; t_0 be the time for the resonance current to pass through the zero time, where $t_0 = \theta_0 / \omega_r$; Q_c be the power switching tube junction capacitance charge; Q_s is the resonant current to the junction capacitance charge supply. According to the equivalent model shown in Fig. 4, it can be obtained that,

$$Q_c = C_j U_{in} \tag{9}$$

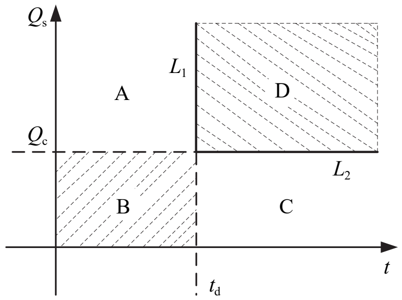

Fig. 6. Distribution figure of operation region.

$$Q_s = \begin{cases} \int_{\frac{T_s}{2}}^{\frac{T_s}{2}+t_d} i_r(t)\mathrm{d}t & \dfrac{\theta_0}{\omega_r} \geqslant t_d \\ \int_{\frac{T_s}{2}}^{\frac{T_s}{2}+\frac{\theta_0}{\omega_r}} i_r(t)\mathrm{d}t & \dfrac{\theta_0}{\omega_r} < t_d \end{cases} \tag{10}$$

According to the balanced relationship between the resonant current charge supply and the switching tube junction capacitance charge demand, as well as the magnitude relationship between the current over-zero time and the dead time, the converter can be divided into four operating regions, whose distribution diagrams are shown in Fig. 6. The operating principle of each operating region is analyzed in detail below.

Region A ($t_0 < t_d$, $Q_s > Q_c$). At the moment when the resonant current i_r over 0, the drain-source voltage of switching tube Q_1 has dropped to 0 and the anti-parallel diode conducts. However, since the dead time has not yet ended, the resonant network maintains resonance, resulting in the current reversal during the dead time and D_1 cutoff. Since the drive signal has not yet arrived, the resonant current charges C_1 again, causing the voltage to rise continuously and the soft-switching operating conditions to be destroyed. When the drive signal arrives, the voltage at both ends of D_1 is no longer zero, and this region is the non-soft-switching operating region.

Region B ($t_0 < t_d$, $Q_s < Q_c$). At the moment when the resonant current i_r passes 0, the drain-source voltage of switch Q_1 has current i_r passes 0, and the drain-source voltage of switch Q_1 has not yet dropped to 0. During the $t_0 < t_d$ period, the resonant network operates in the same state as that in region A, where the drain-source voltage is recharged before it drops to 0, and soft-switching operating conditions cannot be created. Therefore this region is also a non-soft-switching operating region.

Region C ($t_0 > t_d$, $Q_s < Q_c$). In this region, although the current back to 0 time is greater than the dead time, the amount of charge that can be provided during the dead time is less than the charge demand. Before the drive signal of Q_1 arrives, the drain-source voltage of Q_1 has not dropped to 0, and the soft-switching operating conditions cannot be created. Therefore this region is a non-soft-switching operating region.

Region D ($t_0 > t_d$, $Q_s > Q_c$). The voltage of Q_1 has dropped to 0 during the dead time, and at the end of the dead time, the anti-parallel diode D_1 of Q_1 maintains conduction, which creates the conditions for the soft-switching operation of Q_1. Therefore, this region is the soft-switching operation region.

According to the above analysis, the soft-switching operating region of the LLC resonant converter is region D and the rest is the non-soft-switching operating region, and the demarcation line between the two is the ray L_1 and the ray L_2 (as shown by the thick solid line in Fig. 6). Thus these two rays constitute the soft-switching boundary curve of the LLC resonant converter, and L_1 and L_2 can be expressed as (11) and (12), respectively.

$$\begin{cases} Q_s \geqslant Q_c \\ \dfrac{\theta_0}{\omega_r} = t_d \end{cases} \tag{11}$$

$$\begin{cases} Q_s = Q_c \\ \dfrac{\theta_0}{\omega_r} \geqslant t_d \end{cases} \tag{12}$$

B. Dead Time Design of Three-Phase LLC Resonant Converter

From the boundary analysis of the soft-switching realization in the previous section, it can be seen that in order to realize the ZVS turn-on of the power switching tube, the converter must always work in the above-analyzed region D. If the dead time is too small, the IGBT junction capacitance is not discharged completely, and zero-voltage turn-on can not be realized; if the dead time is too large, the loss will be increased, and it may be out of the soft-switching working condition. After the parameters of the resonant network are determined, the length of the dead time directly determines whether the converter can successfully realize the soft-switching operation within the full design load range. In order to determine the required dead time, the minimum dead time required to realize soft-switching must be considered to ensure that the converter can work in the soft-switching state under the worst condition, which in turn affects the voltage stress of the IGBTs and the efficiency of the converter, and the selection of the dead time is mainly limited by the minimum dead time and the maximum dead time. The first is the determination of the minimum dead time because the parasitic capacitance of the power switching tube must have enough time to be completely discharged during the dead time. As can be seen in Fig. 5 LLC operating waveforms, in i_m through the peak after a very short period of time, it can be assumed that the resonant current value is unchanged, at this time, the power switching tube parasitic capacitance begins to discharge, just when the parasitic dead time when the charge is drained the shortest time. If less than this time, the power switching tube parasitic capacitance has not been completely discharged, can not realize the ZVS open. From the above analysis, to meet the primary power tube ZVS turn on the minimum dead time,

$$t_d \geqslant C_j \frac{\mathrm{d}u}{i_r} \tag{13}$$

where C_j is the parasitic capacitance of the IGBT and $\mathrm{d}u$ is the

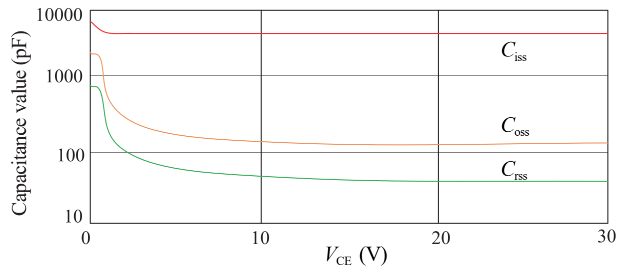

Fig. 7. Relationship between output capacitance and V_{CE}.

differential of the voltage. Minimum dead time to satisfy the turn-on of the primary-side power tube ZVS,

$$t_{\mathrm{dmin}} = C_{\mathrm{j}} \frac{U_{\mathrm{in}}}{i_{\mathrm{m\_pk}}} \tag{14}$$

The maximum dead time must be less than the primary side current reverse over zero time to avoid the output capacitor reverse charging. According to the LLC operating waveform in Fig. 5, it can be seen that at the moment of t_2, the circuit enters the three-element resonant operating state of L_r, C_r, and L_m, and if (15) or (16) is satisfied, the vice-side diode starts to conduct and L_m is clamped. At the moment t_3, the circuit enters the dead time and the parasitic capacitance starts to discharge. At the moment t_5, if the parasitic capacitance is not fully discharged, the power switching tube will lose the ZVS turn-on condition. Therefore, the end of discharging the parasitic capacitance exactly at the moment of t_5 is the critical condition for the ZVS turn-on of the power switching tube, and the maximum dead time is the interval [t_3, t_5].

$$(U_{\mathrm{in}} - U_{\mathrm{Cr}}) \frac{L_{\mathrm{m}}}{L_{\mathrm{m}} + L_{\mathrm{r}}} < -nU_{\mathrm{o}} \tag{15}$$

$$(U_{\mathrm{in}} - U_{\mathrm{Cr}}) \frac{L_{\mathrm{m}}}{L_{\mathrm{m}} + L_{\mathrm{r}}} > nU_{\mathrm{o}} \tag{16}$$

Based on the above analysis, the maximum dead time to satisfy the turn-on of the primary power tube ZVS is obtained.

$$t_{\mathrm{dmin}} = t_{\mathrm{dmin}} + \frac{\tan^{-1}\left(\frac{n^2 U_{\mathrm{o}}^2}{2\pi f_{\mathrm{r}} L_{\mathrm{m}} P_{\mathrm{o}}} \frac{f_{\mathrm{s}}}{f_{\mathrm{r}}}\right)}{2\pi f_{\mathrm{r}}} \tag{17}$$

where P_o is the single-phase output power, and f_r is the series resonant frequency.

IV. Characterization of IGBT Output Capacitance

A. IGBT Output Capacitance

There is a parasitic capacitance between every 2 electrodes of the 3 electrodes of IGBT, which are C_{GE}, C_{GC}, and C_{EC}. The output capacitance C_{oss} of IGBT mainly includes C_{GC} and C_{EC}

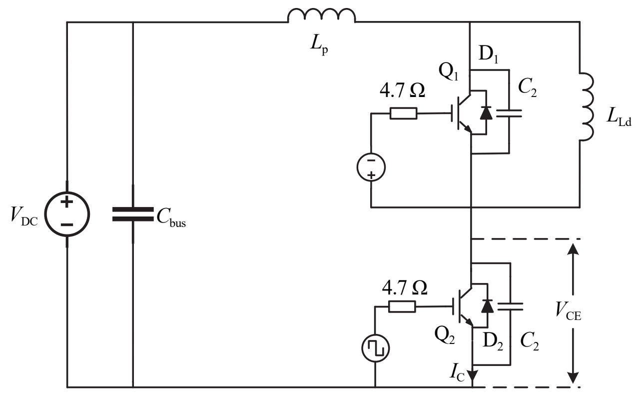

Fig. 8. Double pulse test schematic diagram of the half-bridge IGBT module.

[20]–[21]. The typical IGBT parasitic capacitance versus voltage is shown in Fig. 7.

For the three-phase LLC converter whether it can successfully realize the zero-voltage turn-on of IGBT, the output capacitance value of IGBT is very critical data.

According to the previous section on the maximum and minimum dead time limit analysis, if you want to realize the IGBT zero-voltage turn-on, the same bridge arm between the two IGBT drive signal dead time must be greater than its output capacitance charging and discharging time and is less than the primary side of the current reversal over the zero time. In practice, the IGBT output capacitance size is not a constant value, it will receive V_{CE} and operating temperature. Therefore, when V_{CE} is unchanged, the charging time of IGBT output capacitor C_1 (i.e., the time corresponding to the establishment of Q_1 voltage) will vary with the temperature. If the three-phase LLC dead time is calculated based on the typical value in the technical specifications at room temperature, there is a possibility that the charge on the junction capacitor C_1 has not yet been drained by the resonant current and Q_2 has already been turned on in practical applications, thus losing the ZVS turn-on condition. Therefore, the output capacitance of the IGBT should be determined under the worst operating conditions to determine the required dead time.

B. Analysis of the Effect of Temperature Variation on the Operating Characteristics of IGBTs

The study of IGBT operating characteristics is carried out using the double-pulse test method. The test schematic is shown in Fig. 8, in which L_{Ld} is the load inductance, L_p is the line parasitic inductance, and C_{bus} is the bus capacitance. 2 IGBTs form a half-bridge structure.

The upper tube drive applies a negative voltage to ensure that the IGBTs are turned off. In contrast, the lower tube applies a normal drive signal to observe the voltage buildup and current decay characteristics of the lower tube when it is turned off [22]–[23]. Table I shows the parameters of the IGBT test setup.

According to the subsequent prototype parameters bus voltage V_{DC} = 800 V, the on-state current of the IGBT is set at 20 A,

TABLE I
Parameters of the IGBT Test Device

Component	Parameter
Bus capacitance C_{bus} (μF)	2340
Load inductance L_{Ld} (μH)	150
Parasitic inductance L_p (nH)	140

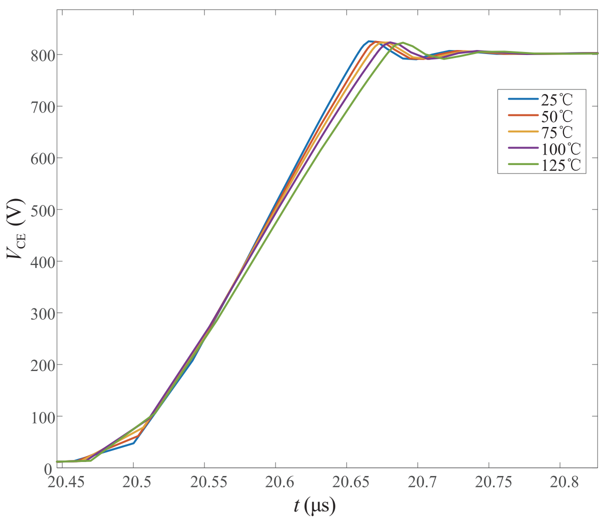

Fig. 9. Turn off voltage waveforms of IGBT at different junction temperatures.

and the temperature of the thermostat box starts from 25 °C, and 1 double-pulse test is carried out for every 25 °C of temperature rise to obtain the waveforms of the voltage at both ends of the IGBTs between the C-pole and the E-pole at different temperatures as shown in Fig. 9.

From Fig. 9, it can be seen that with the same bus voltage and collector current, the dv/dt decreases and the voltage build-up time grows as the junction temperature increases. Finally, the junction capacitance of the IGBT corresponding to the highest junction temperature is used as a reference for the setting of the dead time, and the worst-case junction capacitance size is determined to be 4.5 nF.

V. Experimental Verification

To verify the accuracy of the proposed theory, a 100 kW three-phase bidirectional LLC resonant converter prototype is designed in this paper with the parameters shown in Table II, and the physical diagram of the prototype is shown in Fig. 10.

During the operation of the LLC circuit, the IGBT output capacitance must be selected according to the maximum value to ensure that the IGBT achieves zero-voltage turn-on in the full temperature range so that the IGBT output capacitor voltage can be discharged to 0 V. The IGBT output capacitance is also selected according to the maximum value. In the worst operating conditions (i.e., the highest operating temperature), the IGBT output capacitance of 4.5 nF, so that the calculation of the dead time selection range of 0.482 μs < t_d < 1.252 μs, in practice, t_{dmin} will be with the temperature and load current

TABLE II
Parameters of the Prototype

Component	Parameter
Power rating P_o (kW)	100
Input voltage U_{in} (V)	800
Output voltage U_o (V)	600
Resonant inductance L_r (μH)	8.5
Excitation inductance L_m (μH)	715.5
Resonant capacitance C_r (μF)	9.4
Switching frequency f_s (kHz)	17
Ratio n	1.333

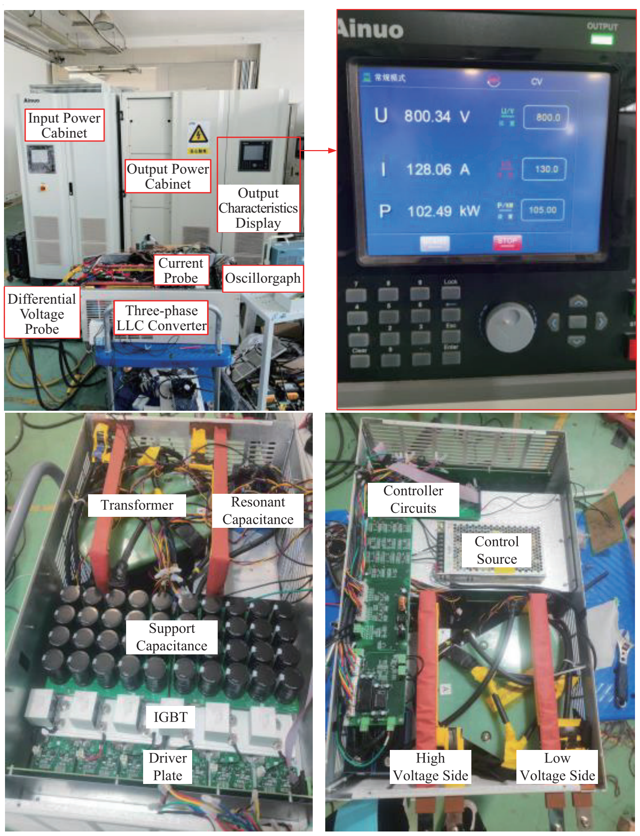

Fig. 10. Efficiency test and experiment platform.

changes, but also to take into account the deviation of the excitation inductance manufacturing and measurement error, so the actual charging and discharging time than the theoretical calculation of the value of the larger, the actual take the dead time. Considering a certain margin, the actual dead time is t_d = 1.1 μs.

The primary-side PWM drive waveform of the three-phase LLC converter prototype is shown in Fig. 11. From the figure, it can be seen that phase A exceeds phase B by one-third of the cycle, and phase B exceeds phase C by one-third of the cycle. Three-phase drive phase difference of 120°, and in each phase of the power switching tube drive there is a certain dead time to meet the drive requirements.

The optimized design dead time t_d=1.1 μs, based on [12]

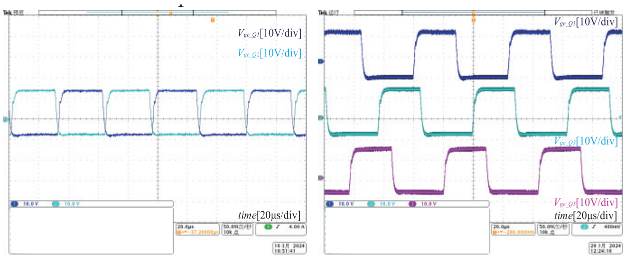

(a) (b)

Fig. 11. Three-phase LLC drive waveform. (a) A-phase bridge arm up and down tube driving waveforms. (b) Three-phase driving waveform.

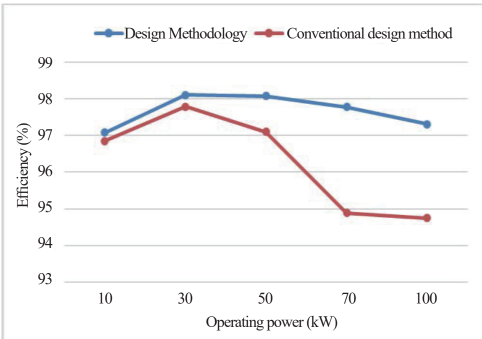

Fig. 12. Efficiency curve comparison chart.

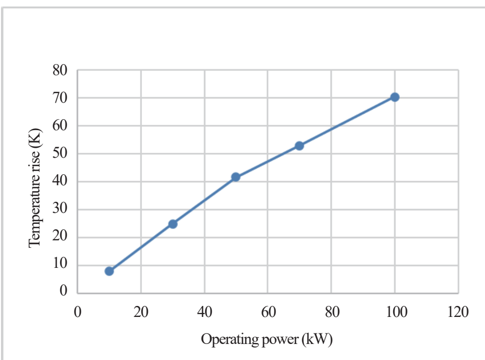

Fig. 13. Working temperature change of prototype.

under the traditional design of the dead time $t_d = 0.8$ μs. Determine the efficiency of the two groups under different power at the rated voltage and the temperature rise of the prototype at an ambient temperature of 25 °C, plot the efficiency comparison curve of the two groups as shown in Fig. 12, and the approximate temperature rise curve of the prototype operation as shown in Fig. 13. The experimental temperature rise diagram of the three-phase LLC resonant converter prototype is shown in Fig. 14. The three-phase LLC prototype startup voltage and current waveforms are shown in Fig. 15, where the dark blue waveform is the input voltage, the light blue waveform is the output voltage, the red waveform is the C-phase resonant current waveform, and the green waveform is the output current waveform.

Analysis of the plotted curve can be seen, in the prototype load is small prototype work stability when the temperature

(a) (b)

Fig. 14. Photograph of temperature rise of three-phase LLC converter prototype. (a) Starting temperature. (b) Final temperature.

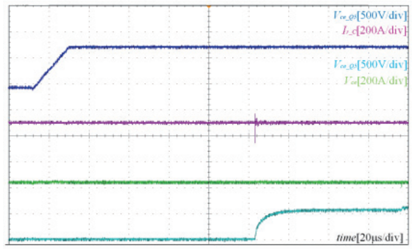

Fig. 15. Three-phase LLC prototype startup voltage and current waveforms.

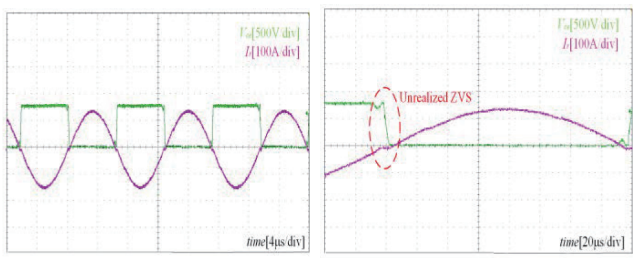

(a) (b)

Fig. 16. The prototype loses the soft switching waveform in the traditional design. (a) Power-switching tube soft-switching waveform. (b) Soft-switching detail waveform.

rise is also small, this time the dead time design method proposed in this paper and the traditional dead time design method to get the prototype efficiency is not much difference. In the prototype load aggravation when the IGBT operating temperature becomes high, the IGBT operating characteristics have changed, resulting in the dead time setting being unreasonable, the IGBT lost the soft switching characteristics, as shown in Fig. 16 using the traditional dead time design method of the soft switching characteristics of the waveform, resulting in a great decline in the efficiency of the prototype, the traditional design method compared to this paper's design method, the efficiency of the prototype decreased by 2.5%.

The dead time half-load and full-load operation circuit under the design method in this paper reaches a steady state when the C-phase power switch turn-on voltage and turn-on current signals are shown in Fig. 17, from Fig. 17, it can be seen that in the full load range of the power switch voltage is reduced to 0 before the current begins to increase, the power switch to achieve the ZVS turn-on. Therefore, it can be seen that the dead time optimization method proposed in this paper can still

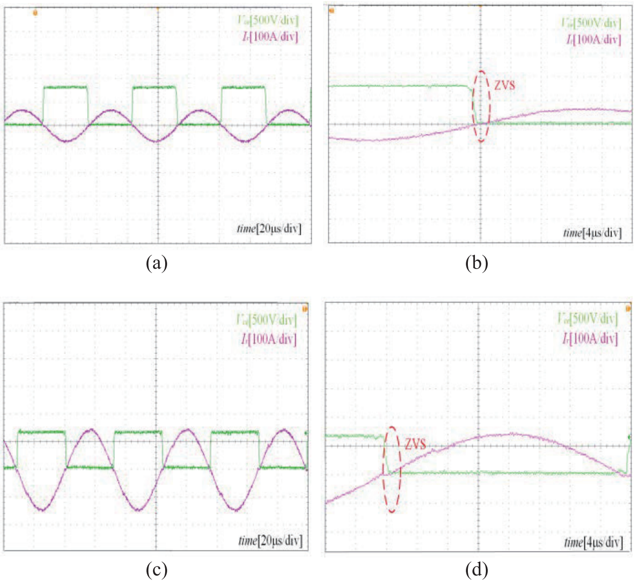

Fig. 17. Realized waveforms of the prototype ZVS under the design methodology of this paper. (a) Full load waveform. (b) Detailed view of full load ZVS waveform. (c) Half load waveform. (d) Detailed view of half-load ZVS waveform.

achieve soft switching and improve the converter's efficiency when the IGBT's operating temperature is high after the workload is aggravated.

In summary, the nonlinear effects of operating temperature and current on the IGBT output capacitance need to be considered in the actual product design. The dead time design needs to be theoretically calculated under the highest junction temperature of the IGBT and the maximum load condition and finally adjusted finely through the test, to ensure that the IGBT can realize soft switching in the full temperature range and the full load range.

VI. Conclusion

In this paper, the operating principle of the three-phase LLC circuit is analyzed, the equivalent model of the converter operating at the resonance point is established and the original and secondary resonant currents are calculated. On this basis, the soft-switching realization range of the switching tubes of the LLC converter is analyzed. The converter is divided into four operating regions in the full input voltage and full load range, of which three are non-soft-switching operating regions, which need to be avoided in the design process. Then this paper analyzes the relationship between the dead time and soft-switching realization of the LLC converter and deduces the mathematical expressions for the maximum and minimum dead times. Then, based on the problem that the ambient temperature in engineering practice will make the IGBT output capacitance undergo a nonlinear transformation, the operating characteristics of IGBT are analyzed, the worst operating condition of the output capacitance is determined, and the dead time setting formula is corrected to make it more in line with engineering practice. Finally, a three-phase LLC converter prototype is constructed to verify the accuracy of the dead time setting method in this paper. This will help promote the three-phase LLC resonant soft-switching technology to realize a wide range of applications in high-power converters.

References

[1] X. Xia, C. Gong, J. Bao, G. Zhu, and Z. Wang, “LLC resonant converter topology with wide gain and high efficiency,” in *Power System Protection and Control*, vol. 51, no. 3, pp. 99–107, Feb. 2023.

[2] X. Zhu, K. Liu, K. Ye, L. Jiang, and K. Jin, “Isolated bidirectional hybrid LLC converter based on SiC MOSFET,” in *Transactions of China Electrotechnical Society*, vol. 37, no. 16, pp. 4143–4154, Aug. 2022.

[3] Y. Shen, W. Zhao, Z. Chen, and C. Cai, “Full-bridge LLC resonant converter with series-parallel connected transformers for electric vehicle on-board charger,” in *IEEE Access*, vol. 6, pp. 13490–13500, 2018.

[4] H. Zhang, M. Han, X. Zhang, and H. Liu, “Interleaved parallel current sharing control for multi-channel LLC resonant converter,” in *Electric Power Automation Equipment*, vol. 43, no. 4, pp. 62–68, Apr. 2023.

[5] Z. Chen, K. Chen, X. Xiong, and R. He, “Variable frequency interleaved parallel LLC resonant converter based on variable inductor,” in *Electric Machines and Control*, vol. 24, no.12, pp. 97–105, Jun. 2020.

[6] Y. Yang, H. Wu, and T. Guan, “Magnetic integrated current sharing characteristics of interleaved LLC resonant converter,” in *Transactions of China Electrotechnical Society*, vol. 34, no. 12, pp. 2529–2538, Jun. 2019.

[7] X. Feng, S. Wang, G. Zhou, and W. Ma, “Current sharing control strategy of three-phase interleaved paralleled LLC resonant converter based on phase-shifting control,” in *Electric Power Automation Equipment*, vol. 41, no. 12, pp. 166–171, Dec. 2021.

[8] X. Feng, K. Shao, X. Cui, W. Ma, and Y. Wang, “Control strategy of wide voltage gain LLC resonant converter based on multi-mode switching,” in *Transactions of China Electrotechnical Society*, vol. 35, no. 20, pp. 4350–4360, Oct. 2020.

[9] Y. Nakakohara, H. Otake, T. M. Evans, T. Yoshida, M. Tsuruya, and K. Nakahara, “Three-phase LLC series resonant DC/DC converter using SiC MOSFETs to realize high-voltage and high-frequency operation,” in *IEEE Transactions on Industrial Electronics*, vol. 63, no. 4, pp. 2103–2110, Apr. 2016.

[10] R. Beiranvand, B. Rashidian, M. R. Zolghadri, and S. M. H. Alavi, “Designing an adjustable wide range regulated current source,” in *IEEE Transactions on Power Electronics*, vol. 25, no. 1, pp. 197–208, Jan. 2010.

[11] Y. Yuan and D. Xiang, “Study on effects of different factors on IGBT thermal sensitive electrical parameter dV/dt,” in *Journal of Power Supply*, vol. 14, no. 6, pp. 35–39, 66, Dec. 2016.

[12] R. Ren, F. Zhang, and S. Liu, “Optimal design for efficiency based on the dead time and magnetizing inductance of LLC DC transformer,” in *Transactions of China Electrotechnical Society*, vol. 29, no. 10, pp. 141–146, May 2014.

[13] Z. Lv, X. Yan, L. Sun, and W. Fan, “Selection and calculation of LLC converter dead-time considering turn-off transient of MOSFET,” in *Electric Power Automation Equipment*, vol. 37, no. 3, pp. 175–183, Mar. 2017.

[14] P. Ban, Y. Xie, and Z. Wang, “Design of magnetic integrated LLC converter considering dead time,” in *Journal of Magnetic Materials and Devices*, vol. 54, no. 1, pp. 30–35, Jan. 2023.

[15] C. Sun, Q. Sun, R. Wang, Y. Li, and D. Ma, “Adaptive dead-time modulation scheme for bidirectional LLC resonant converter in energy router,” in *CSEE Journal of Power and Energy Systems*, vol. 10, no. 4, pp. 1710–1721, Jul. 2024.

[16] J. Tang, P. Rao, W. Xie, and S. Chen, “Robustness design of LLC resonant converter,” in *Control and Information Technology*, no. 2, pp. 64–71, 86, 2019.

[17] Y. Sun, Z. Deng, G. Xu, G. Deng, Q. Ouyang, and M. Su, “ZVS analysis and design for half bridge bidirectional LLC-DCX converter with consideration of nonlinear capacitance and different load under synchronous turn-on and turn-off modulation,” in *IEEE Transactions on*

Transportation Electrification, vol. 8, no. 2, pp. 2429–2443, Jun. 2022.

[18] M. Noah, S. Kimura, J. Imaoka, W. Martinez, S. Endo, M. Yamamoto, and K. Umetani, "Magnetic design and experimental evaluation of a commercially available single integrated transformer in three-phase LLC resonant converter," in *IEEE Transactions on Industry Applications*, vol. 54, no. 6, pp. 6190–6204, Nov.-Dec. 2018.

[19] H. Cao, Y. Liu, and Y. Wang, "Research on three phase LLC resonant converter, in *Low Voltage Apparatus*, no. 8, pp. 53–59, 2019.

[20] H. Huang, H. Tong, N. Wang, and T. Lu, "Analysis of the influence of IGBT segmented transient model with parasitic oscillation on electromagnetic interference prediction," in *Transactions of China Electrotechnical Society*, vol. 36, no. 12, pp. 2434–2445, Jun. 2021.

[21] B. Wang, W. Zhang, Z. Chen, and Z. Wang, "Wide-band equivalent circuit model of IGBT based on PSPICE," in *Chinese Journal of Power Sources*, no. 12, pp. 2320–2323, 2014.

[22] P. Sun, H. Luo, Y. Dong, W. Li, and X. He, "Junction temperature extraction of high power IGBT module based on turn-off delay time," in *Proceedings of the CSEE*, vol. 35, no. 13, pp. 3366–3372, Jul. 2015.

[23] S. Liu, Y. Chang, W. Li, H. Yang, and R. Zhao, "Dynamic switching characteristics test platform design and parasitic parameter extraction of press-pack IGBT modules," in *Transactions of China Electrotechnical Society*, vol. 32, no. 22, pp. 50–57, Nov. 2017.

Xianjin Huang was born in Hubei, China in 1980. He received the B.S. degree in electrical engineering, the M.S. degree in power electronics and electric drive, and the Ph.D. degree in traffic engineering from Beijing Jiaotong University, Beijing, China, in 2002, 2005, and 2014, respectively. He is currently an Associate Professor with the School of Electrical Engineering, Beijing Jiaotong University. His research interests include traction converter and power semiconductor application for railway systems.

Hongchao Bai was born in June 1983. He received the M.S. degree in Power Electronics and Power Drives from Beihang University in 2007. He is a Senior Engineer and is engaged in the research on converter topologies and their control characteristics as well as the research on the topological characteristics of bidirectional power supplies.

Zhidong Xue was born in Shijiazhuang, China, in 2000. He received the B.Eng. degree in electrical engineering from Beijing Jiaotong University, China, in 2022. His research direction is efficiency optimization design and control method design of bidirectional DC/DC converter.

Yinghui Zhao was born in December 1981. He received the M.S. degree in Communication and Information Systems from Southwest Jiaotong University in 2006. He is a Senior Engineer and a Member of the Chinese Society for Electrical Engineering. His main research focuses on DC-DC topologies and their control as well as bidirectional power systems.

Wenwen Shi was born in November 1992. He received the M.S. degree in Power Electronics and Power Drives from Harbin University of Science and Technology in 2019. He is an Engineer and a Member of the Chinese Society for Electrical Engineering. His main research focuses on AC power supply topologies and their control, linear power amplifiers and precision measurement systems.

Zhao Linfeng was born in Liaoning, China, in 2000. He received the B.Eng. degree in electrical engineering from Hefei University of Technology, China, in 2023. His research directions are the efficiency optimization research of bidirectional converters and the research on radio frequency power supplies.